

## Dynamical Effects in Resonant X-Ray Diffraction

S. Macke,<sup>1,2</sup> J. E. Hamann-Borrero,<sup>3</sup> R. J. Green,<sup>1,4</sup> B. Keimer,<sup>2</sup> G. A. Sawatzky,<sup>1</sup> and M. W. Haverkort<sup>1,4</sup>

<sup>1</sup>Quantum Matter Institute, Physics and Astronomy Department, The Brimacombe Building, 2355 East Mall, Vancouver V6T 1Z4, Canada

<sup>2</sup>Max Planck Institute for Solid State Research, Heisenbergstraße 1, 70569 Stuttgart, Germany

<sup>3</sup>Leibniz Institute for Solid State and Materials Research Dresden, Helmholtzstraße 20, 01069 Dresden, Germany

<sup>4</sup>Max Planck Institute for Chemical Physics of Solids, Nöthnitzer Straße 40, 01187 Dresden, Germany

(Received 31 May 2016; published 7 September 2016)

Using resonant magnetic diffraction at the Ni  $L_{2,3}$  edge in a  $\text{LaNiO}_3$  superlattice, we show that dynamical effects beyond the standard kinematic approximation can drastically modify the resonant scattering cross section. In particular, the combination of extinction and refraction convert maxima to minima in the azimuthal-angle dependence of the diffracted intensity, which is commonly used to determine orbital and magnetic structures by resonant x-ray diffraction. We provide a comprehensive theoretical description of these effects by numerically solving Maxwell's equations in three dimensions. The understanding and description of dynamical diffraction enhances the capabilities of resonant x-ray scattering as a probe of electronic ordering phenomena in solids.

DOI: 10.1103/PhysRevLett.117.115501

Resonant x-ray diffraction is a powerful tool for the determination of complex ordering phenomena in transition metal and rare-earth compounds [1]. For off-resonant energies all electrons contribute equally to the scattered intensity. By tuning the energy of the incident photon, one can pick element-specific resonances, thereby enhancing the sensitivity to electronically active elements. The transition metal  $L_{2,3}$  edges ( $2p$  to  $3d$ ) and rare-earth  $M_{4,5}$  edges ( $3d$  to  $4f$ ) belong to the strongest resonances in the x-ray regime, with scattering as strong as  $\approx 800$  electrons per atom at the La  $M_4$  edge. This element-specific enhancement has become a standard method in many different research areas including structure determination of metal centers in large metalloproteins [2] and thin film or interface physics [3,4].

The transition metal  $L_{2,3}$  resonance involves the partially filled transition metal valence shell, which is responsible for many of the intriguing properties of this class of materials. Because of the strict dipole selection rules, the atomic scattering factor at resonance is sensitive to the local electronic structure, including the valence and spin state. Using the polarization dependence of the atomic scattering factor, one gains sensitivity to orbital occupation and ordering, and thus obtains information about which orbitals participate in the transition metal ligand bonding and the exchange interactions between magnetic atoms. Further, the large spin-orbit coupling of the  $2p$  core electrons in  $3d$  transition metal ions results in sizable magneto-optical effects, enabling magnetic diffraction with great sensitivity. At the Ni  $L_{2,3}$  edge the atomic magnetic scattering factor is of the same order of magnitude as the nonmagnetic scattering factor (Fig. 1). This is especially important for magnetic structure determination in thin-film structures that are not amenable to neutron diffraction.

The atomic scattering factors at the transition metal  $L_{2,3}$  or rare-earth  $M_{4,5}$  edges are relatively well understood, even in highly complex materials. For weakly correlated materials they can be calculated using density functional theory [5–7]. For insulating materials the large core-valence interaction creates strongly bound excitons which can be calculated using local models [8,9]. Furthermore, one can expand the total scattering factor in the magnetization, which simplifies using symmetry arguments [10]. In cubic symmetry this yields, up to linear order in the magnetization vector  $\vec{M}$ , the relation [11–14]

$$f_j(\omega, \vec{\epsilon}_i, \vec{\epsilon}_o) = f_j^{(0)}(\omega) \vec{\epsilon}_i \cdot \vec{\epsilon}_o^* + f_j^{(1)}(\omega) \vec{\epsilon}_i \times \vec{\epsilon}_o^* \cdot \vec{M}_j, \quad (1)$$

where  $f_j$  is the atomic scattering factor of site  $j$ ,  $\omega$  is the energy of the scattered photon,  $\vec{\epsilon}_{i(o)}$  is the incoming

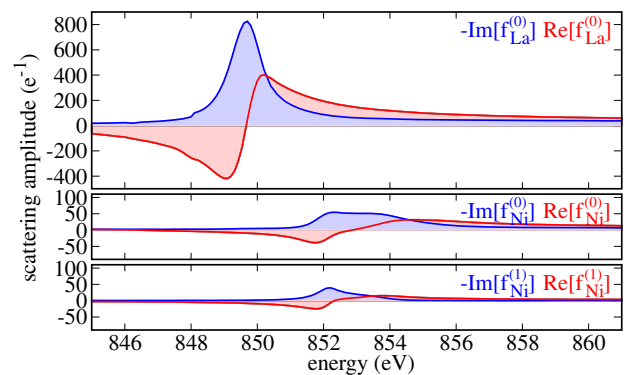


FIG. 1. Real and imaginary parts of the atomic scattering factors of La and Ni as defined in Eq. (1).

(outgoing) polarization vector, and  $f_j^{(k)}(\omega)$  is the atom-specific, polarization- and magnetization-independent, but energy-dependent, scattering factor of site  $j$ .

In the kinematic approximation the total scattered intensity is given as the Fourier transform of the atomic scattering factors:

$$I(\omega, \vec{e}_i, \vec{e}_o) = \left| \sum_j e^{i\vec{q}\cdot\vec{r}_j} f_j(\omega, \vec{e}_i, \vec{e}_o) \right|^2, \quad (2)$$

with  $\vec{q}$  the transferred momentum and  $\vec{r}_j$  the position of atom  $j$  with scattering factor  $f_j(\omega, \vec{e}_i, \vec{e}_o)$ . By varying the resonant energy as well as the incoming polarization, one can in principle determine the complete magnetic orientation at  $\vec{q}$  ( $\vec{M}(\vec{q}) = \sum_j e^{i\vec{q}\cdot\vec{r}_j} \vec{M}_j$ ) in absolute units [12–14]. As inverting the equations from measured intensity to electronic and magnetic structure is challenging, one generally assumes a model and optimizes the model parameters to fit the measured data.

The most commonly practiced method in magnetic structure determination with resonant x rays is the so-called “azimuthal scan”; that is, the scattered intensity is measured as a function of incoming polarization by rotating the crystal around the  $\vec{q}$  vector. Since the raw intensity profiles are often seemingly in contradiction to the relations in Eq. (1), it is common to measure azimuthal scans for two different incoming polarizations,  $\sigma$  and  $\pi$ , and evaluate only the ratio ( $\pi/\sigma$ ) or asymmetry  $[(\pi - \sigma)/(\pi + \sigma)]$  between these signals [15–20]. Here,  $\sigma$  ( $\pi$ ) polarization is defined such that the polarization vector of the light is perpendicular (parallel) to the scattering plane. Measuring these ratios is a practical solution that allows one to extract useful information from polarization-dependent resonant scattering experiments. However, by doing so it makes fits of assumed models to the experimental data less unique. Furthermore, one loses the option to relate the scattered intensity to  $\vec{M}(\vec{q})$  in absolute units. In contrast to neutron diffraction, most resonant x-ray diffraction experiments yield only the orientation, and not the absolute magnitude of ordered magnetic moments in solids.

In resonant x-ray reflectivity experiments, where only a single component of the momentum transfer is varied, it has been well recognized that dynamical effects beyond the kinematic approximation can play an important role [3,21–25]. The atomic scattering factor at resonance can be so large that one needs to consider the reduction of the incoming beam intensity due to extinction, i.e., absorption and scattering. As absorption and scattering can be strongly polarization dependent, this can lead to an effective rotation of the polarization of the incoming beam inside the sample, routing the scattered intensity into otherwise forbidden channels ( $\sigma - \sigma$  scattering of magnetic order) [26–30]. Besides absorption effects, refraction results in an effective propagation direction of the light inside the sample that is

slightly different from the propagation direction of the light outside the sample, so that one measures at slightly different momentum transfer directions than one would naively assume. As the index of refraction is polarization and energy dependent, one finds that the vacuum momentum transfer to fulfill the Bragg conditions changes as a function of polarization and energy. The observed dynamical effects actually stabilize unique solutions to (electronic) structure determinations in several thin-film related experiments [3,25]. The energy-dependent refraction due to the real part of the resonant form factor and its interference with the nonresonant contribution leads to specific dispersing energy-dependent profiles that make the inversion from scattered intensity to magnetic, electronic or chemical profile better defined.

Most three-dimensional resonant x-ray diffraction experiments, on the other hand, are analyzed using kinematic models [15–20,27,31–38]. Several dynamical effects in diffraction have been reported [39], but off resonance these are often small corrections to the kinematic approximation. On resonance, where the optical constants are much larger, one should expect dynamical effects in diffraction to be of the same order of magnitude as found in reflectivity. However, a systematic treatment of dynamical resonant x-ray diffraction has thus far not been available.

The theoretical treatment of resonant diffraction is far more complex than the description of resonant reflectivity. In reflectivity the scattered momentum is perpendicular to the sample surface, and the scattered wave has infinite wavelength in the direction parallel to the surface. This results in an effective one-dimensional problem, for which great simplifications can be made to the solution of Maxwell’s equations [40]. In particular, one can assume an effective medium perpendicular to the surface. In order to calculate resonant x-ray diffraction, one needs to solve Maxwell’s equations in three dimensions in a solid where each atom has an atomic scattering factor given by a general three-by-three matrix, which describes how light with incoming polarization  $\vec{e}_i$  scatters into light of polarization  $\vec{e}_o$ .

We have solved the Maxwell equations using a layered Korringa-Kohn-Rostoker (KKR) multiple scattering algorithm [41,42], a method well known to solve the Schrödinger equation in density functional theory. The largest difference compared to traditional KKR implementations for density functional theory is that photons have a polarization, i.e., they are represented by a vector field, whereas electrons are represented by a scalar (charge density). For single atom scattering our solutions reduce to the well-known formulas of Mie scattering. For slabs or crystals they reproduce photonic crystal calculations [43,44] as well as several known dynamical effects in diffraction of isotropic media [45–54]. Unique to our code is that it treats dynamical diffraction using the full general atomic scattering tensors needed for crystals with noncubic crystal symmetry and possible large

magneto-optical effects. It thus can handle dynamical diffraction of orbital and magnetic order including linear magnetic dichroism. The implementation is available in the program QUAD (quantitative diffraction) [55]. The result is a program optimized for maximum scalability and flexibility that is able to describe many different dynamical diffraction experiments.

To illustrate the importance of dynamical effects in resonant diffraction and the capability of the QUAD program in describing these effects, we now consider magnetic Bragg diffraction from a  $[(\text{LaNiO}_3)_2/(\text{LaAlO}_3)_2]_{46}$  superlattice, and compare calculations in the kinematic and dynamical approximation to experimental data taken from Ref. [17]. Rare-earth nickelates exhibit a manifold of complex charge and spin ordering phenomena which can be tuned using temperature, strain, or dimensionality, i.e., sandwiching ultrathin films between insulating layers [17,23,37]. Because of the large valence, spin, and orbital-dependent atomic scattering factors at the Ni  $L$  edge, resonant x-ray diffraction is an effective tool to elucidate these phenomena.

To calculate the resonant diffraction, one needs the energy-dependent atomic scattering factors. For  $f^{(0)}(\omega)$  of Ni and La, we used the values of Ref. [25]. The values of  $f^{(1)}$ , as shown in Fig. 1, are calculated using the program package QUANTY [9,56] using a double cluster within the multiplet ligand field theory framework [57]. The  $M$  edges of La with a valence  $3+$  are well known strong scatterers because of their high multiplicity, long lifetime, and empty degenerate  $4f$  shell. The Ni  $L_3$  resonance is slightly higher in energy than the La  $M_4$  resonance, but strong tails of La are still present at the Ni  $L_3$  energy.

The  $[(\text{LaNiO}_3)_2/(\text{LaAlO}_3)_2]_{46}$  superlattice in our investigation has a (001) surface, and the magnetic moments on the Ni sites order with a  $(1/4, 1/4, 1/4)$  Miller index in pseudocubic notation. In the kinematic approximation the scattered intensity is proportional to the projection of the magnetic moment to the cross product of the incoming and outgoing polarization [Eq. (1)]. By varying the polarization vector  $\vec{e}_i$ , this allows one to determine the magnetic ordering. The incoming polarization in sample coordinates is changed by using either  $\sigma$  or  $\pi$  polarized light or by changing the scattering geometry, i.e., rotating the sample around  $\vec{q}$ .

Figure 2(a) shows the diffracted intensity using the magnetic model of Ref. [17] within the kinematic approximation [Eq. (2)]. From  $\psi = 20^\circ$  to  $\psi = 160^\circ$  constructive interference leads to a broad maximum for  $\pi$  polarized incoming light (minimum at  $\psi = 270^\circ$ ). This is in contrast to the experiment (crosses) where the intensity for incoming  $\pi$  polarized light goes down from  $\psi = -30^\circ$  to  $\psi = 50^\circ$  (up from  $\psi = 150^\circ$  to  $\psi = 210^\circ$ ). Adding corrections to the kinematic model to account for a change in probed volume due to changing incident angles, as shown in Fig. 2(b), makes the agreement between theory and experiment

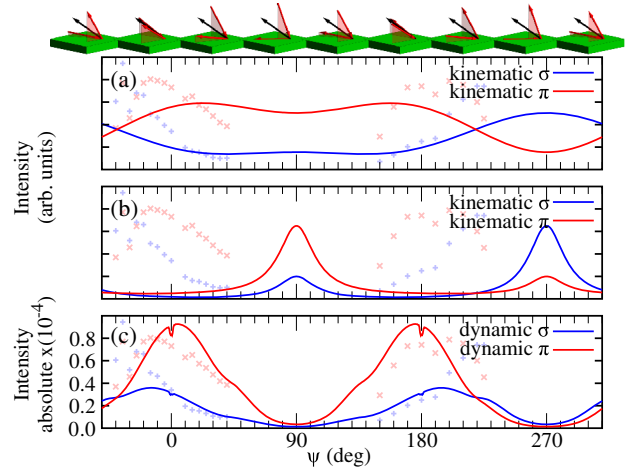


FIG. 2. Normalized diffracted intensity as a function of azimuthal angle (rotation around  $\vec{q}$ ). Calculated intensity within the (a) kinematic approximation, (b) kinematic approximation corrected for the scattered volume, and (c) dynamic approximation. Experimental results from Frano *et al.* [17] are included as crosses. The measured data points below  $\psi = 90^\circ$  are scaled by a factor of 2 to correct for sample alignment. The top panel shows the scattering geometry. The  $(1/4, 1/4, 1/4)$  scattering vector is shown in black, the incoming and outgoing light beams in red.

worse. The inclusion of dynamical effects in the calculation, on the other hand, changes the diffracted intensity drastically, as can be seen in Fig. 2(c). The dynamical calculations are in good agreement with the experimental data. In contrast to kinematical calculations, they accurately reproduce the location of the maxima and minima in the  $\psi$  dependence of the diffracted intensity. They also predict the absolute intensity by which the amplitude of the ordered moment is determined. This requires a careful intensity calibration, which is an interesting challenge for future work.

Many experimental investigations do not use the diffracted intensity for  $\pi$  and  $\sigma$  incoming polarization separately, but instead focus on the intensity ratio, which is less dependent on geometrical factors [15–20]. In Fig. 3 we show this ratio for the kinematic and dynamic approximation and for the measurement. All three curves are in agreement with each other. Nonetheless, differences of the order of 20% can be observed between the calculations in the dynamic or kinematic approximation. One thus needs to be careful when relating deviations from calculations using the kinematic approximation to physical effects in the sample.

In order to understand the difference between the dynamic and kinematic approximation, it is useful to look at a map of the scattered intensity varying both the azimuthal angle as well as the transferred momentum in the  $z$  direction perpendicular to the sample surface (Fig. 4). The white areas around  $\psi = 90^\circ$  and  $\psi = 270^\circ$  are those places where either the outgoing ( $90^\circ$ ) or incoming ( $270^\circ$ ) beam is below the sample horizon. In the kinematic

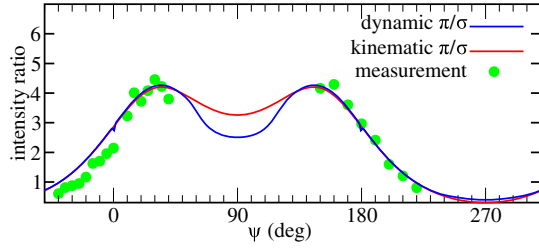


FIG. 3. Diffracted intensity ratio of incoming  $\pi$  and  $\sigma$  polarized light as a function of azimuth angle (rotation around  $\vec{q}$ ). Calculated intensity within the kinematic approximation and dynamic approximation compared to experimental data from Frano *et al.* [17].

approximation one can see that the maxima of the intensity as a function of  $L$  are independent of the azimuthal angle. The intensity as a function of  $L$  and  $\psi$  factors into a function on the azimuthal angle  $\psi$  related to the optical constants and a function of the momentum transfer  $L$  related to the Fourier transform of the atom positions, i.e., the structure factor. The maximum at  $L = 1/4$  originates from the magnetic ordering, whereas the side maxima at a distance of  $\Delta L = 0.0054$  are related to the total sample thickness of  $696 \text{ \AA}$ .

The dynamical calculation of the scattered intensity (top panel of Fig. 4) shows much richer features than the kinematic approximation. The diffraction maximum due to the magnetic ordering at  $(1/4, 1/4, 1/4)$  does not sit at  $L = 1/4$  but at larger values of  $L$ . The  $L$  value to fulfill the Bragg conditions at the  $(1/4, 1/4, 1/4)$  reflection furthermore varies as a function of azimuthal angle. This is related to a change of propagation direction of the light at the sample surface. The index of refraction ( $n$ ) in the x-ray

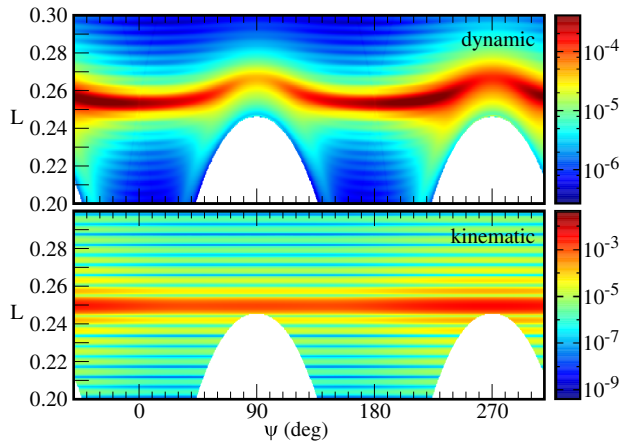


FIG. 4. Calculated diffracted intensity from an  $[(\text{LaNiO}_3)_2/(\text{LaAlO}_3)_2]_{46}$  superlattice for  $\sigma$  polarized incoming light at the Ni  $L_3$  resonance (photon energy  $853 \text{ eV}$ ) as a function of the Miller index  $(1/4, 1/4, L)$  and the azimuthal angle  $\psi$  comparing the kinematic approximation (bottom) to the dynamic approximation (top).

regime is close to 1, but not exactly. At strong resonances the deviation from  $n = 1$  results in sizable refraction and shifts of Bragg peaks by several percent of the reciprocal unit cell. This shift in the scattering angle outside the sample to fulfill the Bragg conditions inside the sample depends on the angle of the ingoing and outgoing beam with the sample surface. At grazing angles the refraction is larger and so is the shift in angles between Bragg conditions inside and outside the sample.

Besides the striking effects of refraction, one notices that the intensity as a function of azimuthal angle  $\psi$  in the dynamic approximation has more features than in the kinematic approximation. Extinction reduces the intensity of the forward beam and thus changes the effective probed volume. The extent of these effects depends on the geometry of the experiment and thus on the azimuthal angle  $\psi$ . It is important to note that refraction does not only happen at the sample surface, but each time the beam hits a layer with different optical constants (for example, changing from  $\text{LaNiO}_3$  to  $\text{LaAlO}_3$ , or from a  $\text{NiO}_2$  layer to a  $\text{LaO}$  layer). Disentangling extinction and refraction due to all planes in the crystal is difficult, because the intensity in the dynamical approximation is a nonlinear function of the atomic scattering factors. It is thus required to consider the full solution of Maxwell's equations for a (periodic) set of atoms, each with their own scattering factor, as we have shown here.

The refraction (change of Bragg position as a function of angle of incidence) and the extinction contain important information about the phase relations of the scattering factors. The real part is more related to refraction, the imaginary part to absorption. This can be important information to distinguish strain waves from charge density modulations [58]. One can gain this additional phase related information by measuring the diffracted signal not using a single point in  $\vec{q}$ , but by using a pixel camera that captures the full Bragg reflection. This would enable one to monitor the movement of the Bragg conditions as one rotates the sample around the  $\vec{q}$  vector.

To conclude, we have implemented a method to treat full dynamical diffraction using arbitrary atomic scattering factors as one encounters in magnetic materials or systems with orbital ordering. The difference between scattered intensity within the dynamic or kinematic approximation can be substantial as exemplified for the magnetic  $(1/4, 1/4, 1/4)$  Bragg reflection in a  $(\text{LaNiO}_3)_2(\text{LaAlO}_3)_2$  superlattice. Dynamical effects can change maxima into minima, move Bragg conditions to different places in  $\vec{q}$ , and thus drastically change the intensity patterns. Dynamical effects are most important for strong resonances, i.e., transition metal  $L_{2,3}$  or rare-earth  $M_{4,5}$  edges. Refraction is most pronounced for grazing angles between the ingoing or outgoing light and the sample surface. From reflectivity measurements it is well known that dynamical effects still play an important role at large incidence angles [3,21–25]. Moreover, for materials

with strong polarization-dependent scattering factors, birefringence can crucially change the observed intensity [26,28]. We find that the ratio of  $\pi$  to  $\sigma$  polarized incoming light is only slightly modified by dynamical effects, validating measurements of the magnetic moment orientation based on this ratio. However, the separate  $\pi$  and  $\sigma$  profiles contain important information that is lost in this procedure. In particular, the analytical description of these profiles we have provided, in combination with sufficiently accurate intensity calibrations in suitably designed experiments, should enable measurements of magnetic moment amplitudes in absolute units, an important capability that is currently not available in resonant x-ray diffraction.

We acknowledge discussions with E. Benckiser and A. Frano and financial support by the DFG under Grants No. HA 6470/1-2 and No. SFB/TRR80.

- 
- [1] J. Fink, E. Schierle, E. Weschke, and J. Geck, *Rep. Prog. Phys.* **76**, 056502 (2013).
- [2] J. Karle, *Science* **232**, 837 (1986).
- [3] S. Macke, A. Radi, J.E. Hamann-Borrero, A. Verna, M. Bluschke, S. Brück, E. Goering, R. Sutarto, F. He, G. Cristiani *et al.*, *Adv. Mater.* **26**, 6554 (2014).
- [4] M. Zwiebler, J.E. Hamann-Borrero, M. Vafae, P. Komissinskiy, S. Macke, R. Sutarto, F. He, B. Büchner, G. A. Sawatzky, L. Alff *et al.*, *New J. Phys.* **17**, 083046 (2015).
- [5] O. Bunau and Y. Joly, *J. Phys. Condens. Matter* **21**, 345501 (2009).
- [6] J. J. Rehr, J. J. Kas, M. P. Prange, A. P. Sorini, Y. Takimoto, and F. Vila, *C.R. Phys.* **10**, 548 (2009).
- [7] K. Gilmore, J. Vinson, E. L. Shirley, D. Prendergast, C. D. Pemmaraju, J. J. Kas, F.D. Vila, and J. J. Rehr, *Comput. Phys. Commun.* **197**, 109 (2015).
- [8] B. T. Thole, R. D. Cowan, G. A. Sawatzky, J. Fink, and J. C. Fuggle, *Phys. Rev. B* **31**, 6856 (1985).
- [9] M. W. Haverkort, M. Zwierzycki, and O. K. Andersen, *Phys. Rev. B* **85**, 165113 (2012).
- [10] M. W. Haverkort, N. Hollmann, I. P. Krug, and A. Tanaka, *Phys. Rev. B* **82**, 094403 (2010).
- [11] J. P. Hannon, G. T. Trammell, M. Blume, and D. Gibbs, *Phys. Rev. Lett.* **61**, 1245 (1988).
- [12] B. T. Thole, P. Carra, F. Sette, and G. van der Laan, *Phys. Rev. Lett.* **68**, 1943 (1992).
- [13] P. Carra, B. T. Thole, M. Altarelli, and X. Wang, *Phys. Rev. Lett.* **70**, 694 (1993).
- [14] H. Ott, C. Schüßler-Langeheine, E. Schierle, A. Y. Grigoriev, V. Leiner, H. Zabel, G. Kaindl, and E. Weschke, *Phys. Rev. B* **74**, 094412 (2006).
- [15] P. Leininger, M. Rahlenbeck, M. Raichle, B. Bohnenbuck, A. Maljuk, C. T. Lin, B. Keimer, E. Weschke, E. Schierle, S. Seki *et al.*, *Phys. Rev. B* **81**, 085111 (2010).
- [16] M. A. Hossain, B. Bohnenbuck, Y. D. Chuang, M. W. Haverkort, I. S. Elfimov, A. Tanaka, A. G. Cruz Gonzalez, Z. Hu, H. J. Lin, C. T. Chen *et al.*, *Phys. Rev. B* **86**, 041102 (2012).
- [17] A. Frano, E. Schierle, M. W. Haverkort, Y. Lu, M. Wu, S. Blanco-Canosa, U. Nwankwo, A. V. Boris, P. Wochner, G. Cristiani *et al.*, *Phys. Rev. Lett.* **111**, 106804 (2013).
- [18] R. Comin, R. Sutarto, F. He, E. H. da Silva Neto, L. Chauviere, A. Frano, R. Liang, W. N. Hardy, D. A. Bonn, Y. Yoshida *et al.*, *Nat. Mater.* **14**, 796 (2015).
- [19] Y. W. Windsor, M. Ramakrishnan, L. Rettig, A. Alberca, E. M. Bothschafter, U. Staub, K. Shimamoto, Y. Hu, T. Lippert, and C. W. Schneider, *Phys. Rev. B* **91**, 235144 (2015).
- [20] A. J. Achkar, M. Zwiebler, C. McMahon, and F. He, *Science* **351**, 576 (2016).
- [21] H. Wadati, D. G. Hawthorn, J. Geck, T. Higuchi, Y. Hikita, H. Y. Hwang, L. F. Kourkoutis, D. A. Muller, S. W. Huang, D. J. Huang *et al.*, *J. Appl. Phys.* **106**, 083705 (2009).
- [22] J. Schlappa, C. F. Chang, Z. Hu, E. Schierle, H. Ott, E. Weschke, G. Kaindl, M. Huijben, G. Rijnders, D. H. A. Blank *et al.*, *J. Phys. Condens. Matter* **24**, 035501 (2012).
- [23] E. Benckiser, M. W. Haverkort, S. Brück, E. Goering, S. Macke, A. Frañó, X. Yang, O. K. Andersen, G. Cristiani, H.-U. Habermeier *et al.*, *Nat. Mater.* **10**, 189 (2011).
- [24] S. Smadici, J. C. T. Lee, G. Logvenov, I. Bozovic, and P. Abbamonte, *J. Phys. Condens. Matter* **26**, 025303 (2013).
- [25] S. Macke and E. Goering, *J. Phys. Condens. Matter* **26**, 363201 (2014).
- [26] H. C. Mertins, P. M. Oppeneer, S. Valencia, W. Gudat, F. Senf, and P. R. Bressler, *Phys. Rev. B* **70**, 235106 (2004).
- [27] V. Scagnoli, U. Staub, Y. Bodenthin, R. A. De Souza, M. Garica-Fernández, M. Garganourakis, A. T. Boothroyd, D. Prabhakaran, and S. W. Lovesey, *Science* **332**, 696 (2011).
- [28] Y. Joly, S. P. Collins, S. Grenier, H. C. N. Tolentino, and M. De Santis, *Phys. Rev. B* **86**, 220101 (2012).
- [29] S. W. Lovesey, V. Scagnoli, A. N. Dobrynin, Y. Joly, and S. P. Collins, *J. Phys. Condens. Matter* **26**, 125504 (2014).
- [30] Y. Joly, Y. Tanaka, D. Cabaret, and S. P. Collins, *Phys. Rev. B* **89**, 224108 (2014).
- [31] P. Abbamonte, *Science* **297**, 581 (2002).
- [32] E. Weschke, H. Ott, E. Schierle, C. Schüßler-Langeheine, D. V. Vyalikh, G. Kaindl, V. Leiner, M. Ay, T. Schmitte, H. Zabel *et al.*, *Phys. Rev. Lett.* **93**, 157204 (2004).
- [33] C. Schüßler-Langeheine, J. Schlappa, A. Tanaka, Z. Hu, C. F. Chang, E. Schierle, M. Benomar, H. Ott, E. Weschke, G. Kaindl *et al.*, *Phys. Rev. Lett.* **95**, 156402 (2005).
- [34] B. J. Kim, H. Ohsumi, T. Komesu, S. Sakai, T. Morita, H. Takagi, and T. Arima, *Science* **323**, 1329 (2009).
- [35] B. Bohnenbuck, I. Zegkinoglou, J. Stremper, C. S. Nelson, H. H. Wu, C. Schüßler-Langeheine, M. Reehuis, E. Schierle, P. Leininger, T. Herrmannsdörfer *et al.*, *Phys. Rev. Lett.* **102**, 037205 (2009).
- [36] L. C. Chapon and S. W. Lovesey, *J. Phys. Condens. Matter* **23**, 252201 (2011).
- [37] Y. Bodenthin, U. Staub, C. Piamonteze, M. García-Fernández, M. J. Martínez-Lope, and J. A. Alonso, *J. Phys. Condens. Matter* **23**, 036002 (2011).
- [38] A. Tanaka, C. F. Chang, M. Buchholz, C. Trabant, E. Schierle, J. Schlappa, D. Schmitz, H. Ott, P. Metcalf, L. H. Tjeng *et al.*, *Phys. Rev. Lett.* **108**, 227203 (2012).
- [39] A. Authier, V. Holy, M. Schlenker, J.-P. Guigay, M. Hart, C. Malgrange, N. Kato, H. Klapper, B. K. Tanner,

- J. Baruchel *et al.*, *X-Ray and Neutron Dynamical Diffraction: Theory and Applications* (Springer, New York, 1996).
- [40] L. G. Parratt, *Phys. Rev.* **95**, 359 (1954).
- [41] J. Korringa, *Physica (Amsterdam)* **13**, 392 (1947).
- [42] W. Kohn and N. Rostoker, *Phys. Rev.* **94**, 1111 (1954).
- [43] N. Stefanou, V. Yannopoulos, and A. Modinos, *Comput. Phys. Commun.* **132**, 189 (2000).
- [44] R. Sainidou, N. Stefanou, I. E. Psarobas, and A. Modinos, *Comput. Phys. Commun.* **166**, 197 (2005).
- [45] A. Ulyanenko, *Appl. Phys. A* **66**, 193 (1998).
- [46] S. A. Stepanov, E. A. Kondrashkina, R. Köhler, D. V. Novikov, G. Materlik, and S. M. Durbin, *Phys. Rev. B* **57**, 4829 (1998).
- [47] Y. P. Stetsko, G.-Y. Lin, Y.-S. Huang, C.-H. Chao, and S.-L. Chang, *Phys. Rev. Lett.* **86**, 2026 (2001).
- [48] V. Holy and P. F. Fewster, *J. Phys. D* **36**, A5 (2003).
- [49] X. Huang and M. Dudley, *Acta Crystallogr. Sect. A* **59**, 163 (2003).
- [50] A. Souvorov, T. Ishikawa, A. Y. Nikulin, Y. P. Stetsko, S.-L. Chang, and P. Zaumseil, *Phys. Rev. B* **70**, 224109 (2004).
- [51] S. G. Podorov, N. N. Faleev, K. M. Pavlov, D. M. Paganin, S. A. Stepanov, and E. Förster, *J. Appl. Crystallogr.* **39**, 652 (2006).
- [52] V. M. Kaganer, *Phys. Rev. B* **75**, 245425 (2007).
- [53] H. Yan, J. Maser, A. Macrander, Q. Shen, S. Vogt, G. B. Stephenson, and H. C. Kang, *Phys. Rev. B* **76**, 115438 (2007).
- [54] S. Stepanov and R. Forrest, *J. Appl. Crystallogr.* **41**, 958 (2008).
- [55] <http://quad.x-ray.center>.
- [56] M. W. Haverkort, G. Sangiovanni, P. Hansmann, A. Toschi, Y. Lu, and S. Macke, *Europhys. Lett.* **108**, 57004 (2014).
- [57] R. J. Green, M. W. Haverkort, and G. A. Sawatzky, *arXiv*: 1608.01645.
- [58] P. Abbamonte, *Phys. Rev. B* **74**, 195113 (2006).